IOSR Journal of Mechanical and Civil Engineering (IOSR-JMCE)
e-ISSN: 2278-1684,p-ISSN: 2320-334X, Volume 13, Issue 6 Ver. II (Nov. - Dec. 2016), PP 113-124
www.iosrjournals.org

Effect of Frictional Welding Between Different Stainless-Steel Materials on Their Torsional Properties

Azeen K. Mohammad[1,] Hawro Khalil[2]
[1,2]*Mechanical Department, College of Engineering, Salahaddin University-Erbil*

Abstract: *The aim of the presented study was to investigate the effect of frictional welding between two different stainless steel materials on their torsional properties. The study took two approaches; an experimental approach and a finite element analysis approach. Experimental approach was undertaken out to study the welded Specimens ability to withstand applied torsional moments and to compare the results for specimens welded with different forging pressures, 101.512MPa, 146.629MPa and 225.583MPa; non-welded specimens were also produced and tested. Finite element analysis approach was undertaken to study the generated heat during the process of welding and the heat transfer throughout the specimen as well as generating a heat transfer profile for the welding process.*
Keywords: *Friction Welding, Torsional Properties, Finite Element Analysis*

I. Introduction

Friction welding obtained by frictional heat is a commercial process, which has found several applications with the advancement in technology; examples includes applications in automotive industry such as the manufacturing of valves, drive shafts and gear levers, applications in space parts industry such as radial pump pistons and drill bits, and other applications in which the of materials is required

- either to obtain some desired properties of different materials.
- or to overcome the difficulties of manufacturing single complicated parts.
- or both.

Without the concerns of typical welding failures [1].

Friction welding is classified by the American Welding Society (AWS) as a solid state welding process that produces a weld at temperatures lower than the melting point of the base metals under compressive force contact of work pieces rotating or moving relative to one another, Figure 1, to produce heat and plastically displays material from the faying surfaces [3]. The resulting joint is of forged quality. Under normal conditions, the faying surfaces do not melt.

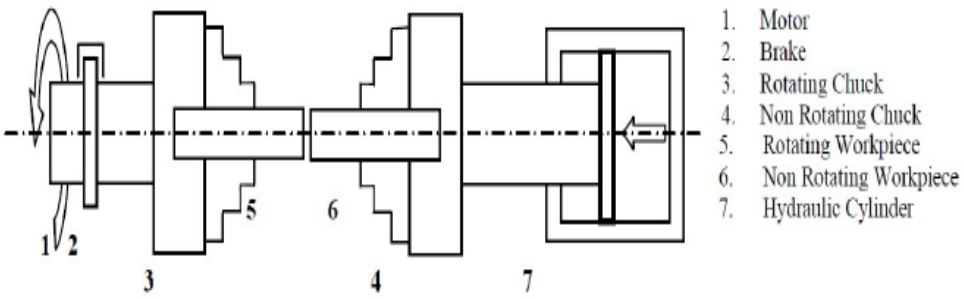

Figure 1: Layout of Continuous Drive Friction Welding [4]

Even metal combinations not normally considered compatible can be joined by friction welding, such as aluminum to steel, copper to aluminum, titanium to copper and nickel alloys to steel, see Table1.As a rule, all metallic engineering materials which are forgeable can be friction welded, including automotive alloys, maraging steel, tool steel, alloy steels and tantalum. In addition, many castings, powder metals and metal matrix composites are weld-able [2].

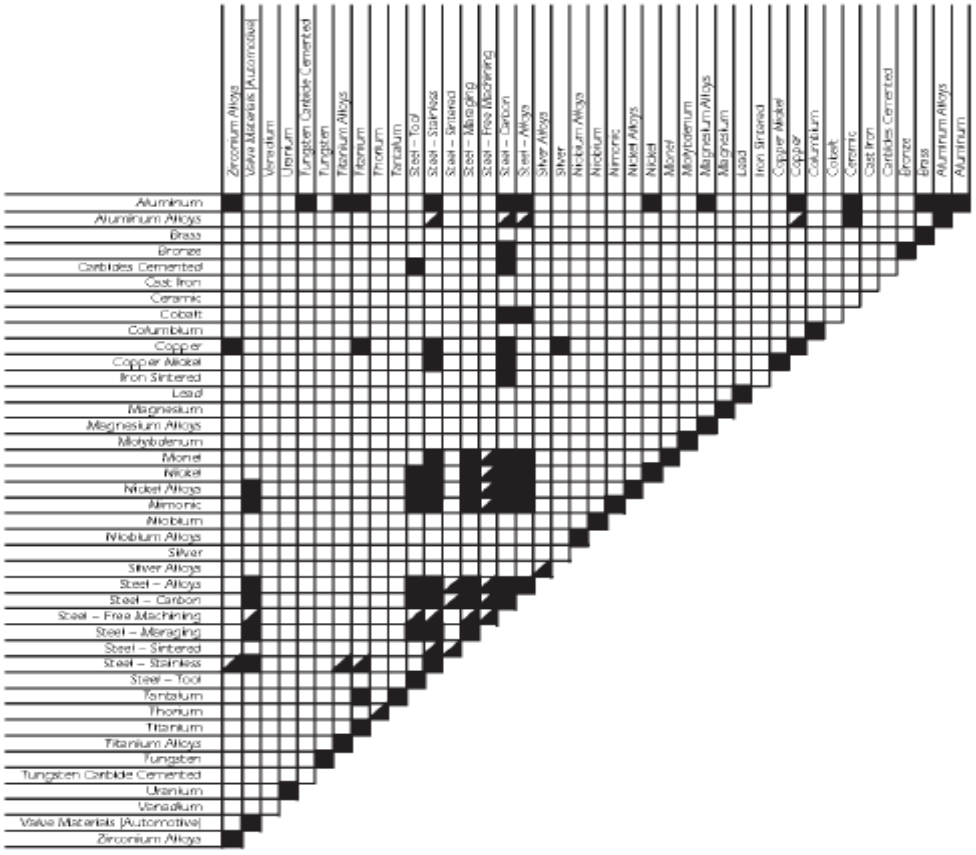

Table 1: Weldable Combinations in Friction Welding

That being said, welded materials are subjected to changes in there mechanical and thermal properties due to the combined act of rubbing, heat generating, pressing, and forging. The highest rate of properties change is mostly found at the locations where the effect of the welding process is maximum, the welded faces, and drops with different rates proportionately to the distance from the welding region as the effect of the welding process decays. The effect of the friction welding between different stainless-steel materials on the torsional properties was investigated in this research. the torsional properties of such welded materials is a main concern as much of the applications includes direct or indirect torsional loads. Having these properties drop down in the welded region introduces a weak point that effects the consideration for future applications. The chemical composition was analyzed for both stainless-steels using a spectrometer. The analysis results for both materials, named $\boldsymbol{\alpha}$ and $\boldsymbol{\beta}$ is shown in Table2 and Table3 respectively. Analysis result showed that the stainless-steel used was a martencite. Figure 2 and 3 shows the micro-structure imaging of both materials.

Table 2: Spectrometer chemical composition for named $\boldsymbol{\alpha}$ Stainless-Steel

	C	Si	Mn	P	S	Cr	Mo	Ni
	%	%	%	%	%	%	%	%
1	0.282	0.345	0.318	0.0100	0.0147	18.01	0.107	1.78
2	0.293	0.337	0.319	0.0094	0.0112	18.15	0.102	1.76
3	0.268	0.327	0.318	0.0096	0.0100	18.18	0.099	1.76
< x > (3)	**0.281**	**0.337**	**0.318**	**0.0096**	**0.0120**	**18.11**	**0.102**	**1.77**
sd	0.0124	0.0091	0.0004	0.0003	0.0024	0.090	0.0040	0.0134
rsd	4.4	2.7	0.1	3.0	20.3	0.5	3.9	0.8

	Al	Co	Cu	Nb	Ti	V	W	Fe
	%	%	%	%	%	%	%	%
1	0.0280	0.050	0.161	< 0.0020	0.0059	0.0199	0.130	78.73
2	0.0274	0.0500	0.166	< 0.0020	0.0057	0.0207	0.120	78.62
3	0.0238	0.051	0.167	< 0.0020	0.0055	0.0200	0.113	78.65
< x > (3)	**0.0264**	**0.050**	**0.165**	**< 0.0020**	**0.0057**	**0.0202**	**0.121**	**78.67**
sd	0.0023	0.0004	0.0032	0.0000	0.0002	0.0005	0.0089	0.057
rsd	8.7	0.8	1.9	0.0	2.7	2.3	7.4	0.1

Table 3: Spectrometer chemical composition for named ***β*** Stainless-Steel

	C	Si	Mn	P	S	Cr	Mo	Ni
	%	%	%	%	%	%	%	%
1	0.246	0.274	0.988	0.0074	0.0176	17.09	0.053	2.20
2	0.237	0.264	1.03	0.0058	0.0136	17.31	0.0495	2.17
3	0.209	0.261	1.03	0.0082	0.0133	17.33	0.0481	2.16
< x > (3)	**0.230**	**0.266**	**1.02**	**0.0071**	**0.0148**	**17.24**	**0.050**	**2.17**
sd	0.0195	0.0070	0.0244	0.0012	0.0024	0.131	0.0025	0.0209
rsd	8.5	2.6	2.4	16.6	16.3	0.8	4.9	1.0

	Al	Co	Cu	Nb	Ti	V	W	Fe
	%	%	%	%	%	%	%	%
1	0.0122	0.0332	0.083	< 0.0020	0.0059	0.0324	< 0.0150	78.94
2	0.0105	0.0330	0.086	< 0.0020	0.0049	0.0293	< 0.0150	78.75
3	0.0048	0.0333	0.086	< 0.0020	0.0054	0.0282	< 0.0150	78.76
< x > (3)	**0.0092**	**0.0332**	**0.085**	**< 0.0020**	**0.0054**	**0.0300**	**< 0.0150**	**78.82**
sd	0.0039	0.0001	0.0016	0.0000	0.0005	0.0022	0.0000	0.105
rsd	42.7	0.4	1.9	0.0	9.2	7.2	0.0	0.1

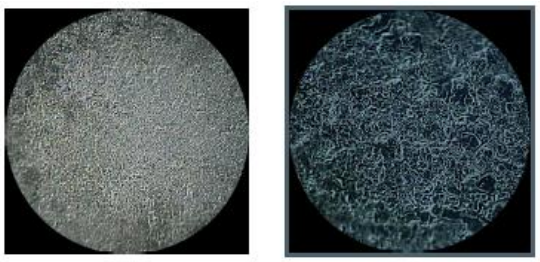

a) 100X b)250X

Figure 2: Micro-structure imaging of ***α*** Stainless-Steel

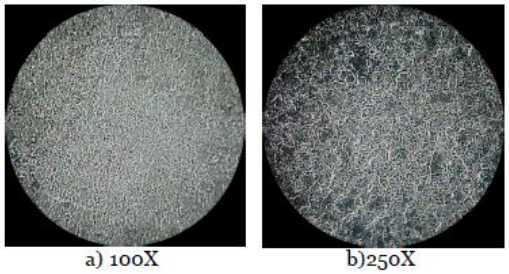

a) 100X b)250X

Figure 3: Micro-structure imaging of ***β*** Stainless-Steel

II. Specimen Preparation and Testing

2.1 Welding

Lath machine, Figure 4, was used for the welding process of prepared cylindrical rods, such approach is widely used due to the convenient and simplicity in addition to the controllability of friction pressure, timing and duration [5][6][7]. One rod was fixed at the non-rotary end and the other was fixed at the rotary end. The non-rotary end has one degree of freedom of moving parallel to the rod's axis of rotation, this movement was manually controlled via screw type motion transmission allowing both motion and pressure control for that part. The rotary end has one degree of freedom of rotating about the rod's axis of rotation. the welding procedure was as follows, Also refer to Figure 5

Figure 4: Lathe Machine

1. Both rods ware tightly fixed as described above.
2. Both rods brought into contact by moving the non-rotary end toward the rotary end, the contact area at the faces to be welded together. The non-rotary end is manually forced to hold the friction pressure during the next step.
3. The rotary end is started, the rotation leads to friction at the contacted surfaces which increases there temperature rapidly.
4. As soon as visual surface redness is confirmed, indicating the temperature rising and the material being forge- able, the friction pressure changes into forging pressure by forcing the non-rotary end against the rotary end. Both surfaces start to forge into each other.
5. Upon visual confirmation of success forging, the rotary end is stopped first while maintaining the forging pressure until no redness is observed at the region of welding.

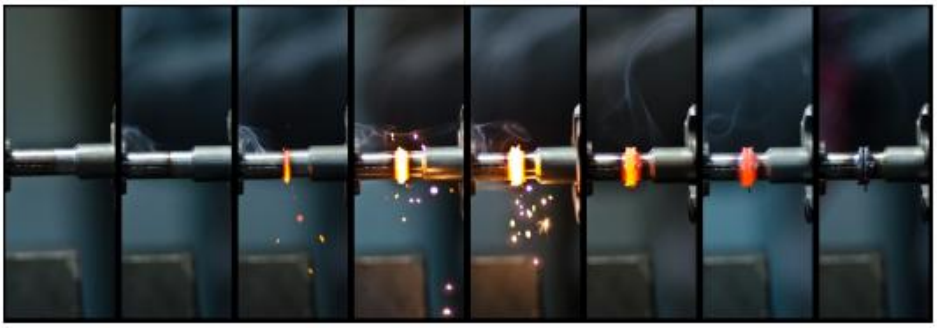

Figure 5: Welding Procedure; the left half has linear movement and the right half has rotational movement.

For including the effect of different **forging pressures** in the study, three welded joints were produced at three different forging pressures. The rotational speed, however, was maintained at 1030*rpm* for each welding process to reduce the number of variables in the study. Additionally, one specimen was produced, in the next section, without welding for each type of Stainless-Steel (i.e. $\boldsymbol{\alpha}$ and $\boldsymbol{\beta}$) for properties examination and evaluation of similar and dissimilar specimen; hence, the total number of specimens was 5. Table 4 includes the details of each weld. Figure 6 shows the welded joints, before machining them into standard specimens.

Specimen No.	1	2	3
Friction Pressure	112.791*MPa*	112.791*MPa*	112.791*MPa*
Friction time	30*min*	30*min*	30*min*
Forging Pressure	101.512*MPa*	146.629*MPa*	225.583*MPa*

Table 4: Friction welding parameters

Figure 6: Welded Joints

2.2 Specimens Machining into Standard Dimensions

After the welded joints where obtained, lathe machine was used to produce standard dimension torsion test specimens, noting that no welding was required for $\boldsymbol{\alpha}$ and $\boldsymbol{\beta}$ specimens. Figure 7 shows a schematic drawing of the specimens. Figure 8 shows the ready-to-test welded specimens.

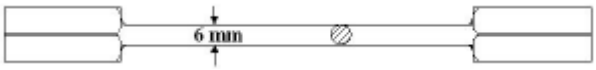

Figure 7: Schematic drawing of the Specimens.

Figure 8: Ready-to-test welded specimens.

2.3 Testing

A manually operated laboratory Torsion-Test instrument was used, Figure9. Torsion load was manually applied via a gearbox which allowed for accurate angular displacement measuring, while the rising torsional stresses within the specimens was monitored using an equipped digital sensor. Due to the dynamic nature of the experiment, counting the angular displacement and recording the resulting stresses in real time while monitoring the specimen behavior could introduce a considerable amount of error and it was found to be a non-practical approach. to eliminate this error, HD DSL camera and sound recording system where used to record the test in real time. The records could be replayed in slow motion to monitor the whole experiment several times and eliminate any inaccuracy in the obtained data.

Figure 9: Laboratory Torsion-Test instrument.

Having the exact same dimension for all specimens meant that calculating the maximum shear stress from the applied torque, Equation 1, was not necessary as the only different variable is the obtained applied torque. For this study, that focuses on comparison rather than absolute values, the applied torque was directly used. The same applies for the strain, found by Equation 2, which was replaced by the direct angular displacement, angle of twist.[8]

$$\tau_{max} = \frac{G.c.\theta}{L} = \frac{T.c}{J} \qquad (1)$$

$$c.\theta$$

Where;
τmax maximum shear stress at the outer surface
γmax maximum shear strain.
T applied torque.
J polar moment of inertia of the cross section.

$$\gamma_{max} = \qquad (2)$$

$$L$$

L length of the object the torque is being applied to or over.
θ angle of twist.
G shear modulus or more commonly the modulus of rigidity.
c radius

III. Finite Element Analysis Set-up and Procedure

One of the major outcomes of the process of friction welding, which can't be practically monitored in real time, is the rising of temperature between the welded faces and the heat transfer through the specimen. The aim of rubbing both faces together is to generate heat as described before; therefore, a part of this study was concerned with how is the temperature generated and the heat is transferred within the specimen during the process of welding. To investigate that, DEFORM Ver.11 FEA tools were used to simulate the friction welding of Stainless- Steel and take a peek at the heat generation and transfer for the whole welded specimen. This method is commonly used when actual data monitoring is non-practical.

3.1 Modeling

DEFORM 3D modeling was used to generate the models, two cylindrical models of the same dimension (24*mm* diameter and 60*mm* height) and same assigned material, martensitic Stainless-Steel. Using 3D models, instead of 2D models, significantly increased the simulation time; however, the 3D models provided much better approximated heat transfer profile for the welding process and gave a three dimensional scoop of the heat generation within the specimens.

3.2 Meshing

As the main aim of this part of the study was to investigate the heat generation and transfer for the whole parts, it was decided that all nodes in the mesh are of equal concern. For this case, equal mesh size was used along with fixed number of elements to uniformly mesh the specimens. Table 5 lists the meshing parameter. The meshed model for one half of the welded joint is shown in figure 10, a small error is introduced to the dimensions after meshing. This error is often encountered in FEA meshing and is negligible in amount for the purpose of this study, it rises from the attempt to split the entire part into the required amount of meshing elements.

DetailedSettings	Remeshcriteria	Summery
Type: System Setup Size Ratio:1	Interference Depth: 0.7Relative Remeshing Method: GlobalRemeshing	Number of Elements: 8000 Number of Nodes:1599Surface Polygons:1682

Table 5: Model Mesh parameters

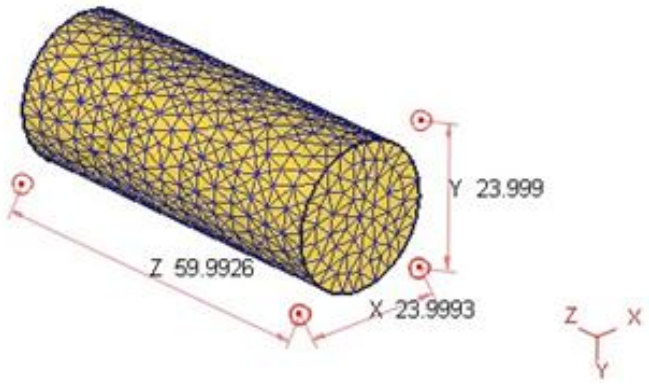

Figure 10: One half meshed model

3.3 Movement and Boundary Conditions

DEFORM used to tools to define motion and force applied to objects, movements and boundary conditions. Using the boundary conditions, one half of the modeled welded joints were fixed by adding a velocity boundary condition of zero in all directions, *X*, *Y* and *Z*. This was only applied to the lower end of this half, where no friction is presented and no movement is expected. The second half didn't had any motion restrains. For this part, a pressing force was applied to the upper end to simulate the friction pressure and the forging pressure. The aim of the FEA study is to visualize the heat transfer in the specimens; hence, via iteration over a scale of different values, a pressure value of 1.3*Mpa* was used in the simulation. In general, it was found that changing the boundary condition and movement values will affect the time for generating the simulations profile, the rate of heat transfer profile or the stress distribution profile as examples. The Movement tools were used to simulate the rotation of the rotating half over a period of time, a rotational speed of 1030*rpm* was defined as movement for the second half.

3.4 Simulation

The simulation was divided into two stages:

1. The first stage simulated the friction pressure without rotation, for a time lapse of 1*sec*
2. The second stage simulated the friction pressure + the rotational speed, the heating process for a time lapse of 10*sec*.

Table 6 lists the simulation parameters:

Table 6: Simulation Parameters

Units	SI
Type	Lagrangian incremental
Mode	Deformation & Heat Transfer
Simulation steps	100 for stage 1, 1000 for stage 2 and 100 for stage
Step increment	$\eth.01sec/step$
Remesh criteria	0.7 Relative
Solver	Conjugate gradient
Iteration method	Direct iteration
Velocity and force error	Default

IV. Results and Discussion

4.1 Testing Results

Figure 11 plots the resulted torque, torsional moment, from the torsion test against the torsional, angular, dis- placement. Table 7 lists the angular displacements θ and torsional moment MT for all five specimens. The final point for each curve, final data, is where the specimen fails, raptures. Specimen 1,2 and 3 curves are for the welded specimens at different forging pressure, while the other two curves are for $\boldsymbol{\alpha}$ and $\boldsymbol{\beta}$ specimen. Figure 12 shows the ruptured location after testing in addition to imaging of the ruptured face for each specimen.

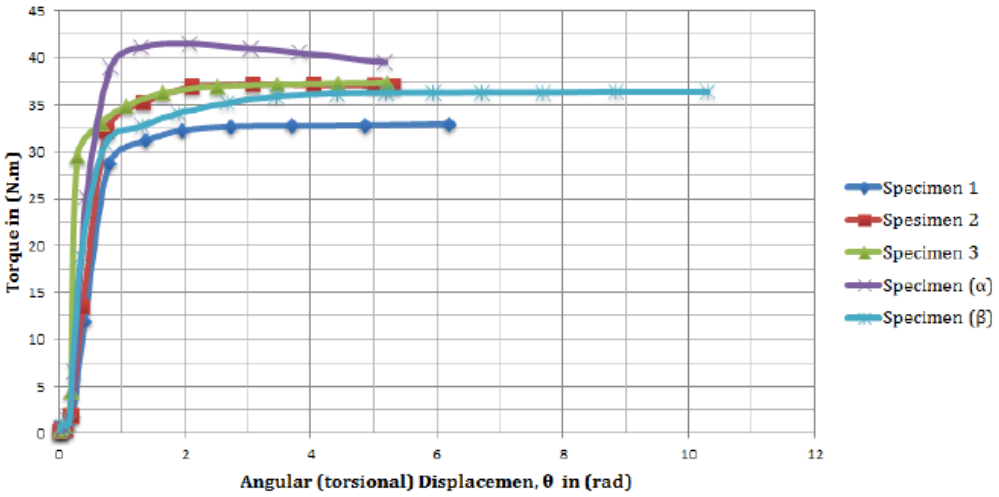

Figure 11: Torsional Displacement - Torque plot for the tested specimens

Table 7: Torsion Test Data: θ in *rad* and MT in *N.m*

Specimen 1		Specimen 2		Specimen 3		Material α		Material β	
θ	M_T	θ	M_T	θ	M_T	θ	M_T	θ	M_T
0.0241	0.2	0.0187	0.1	0.0241	0.3	0.050	0.1	0.0161	0.65
0.0483	0.35	0.0429	0.45	0.0483	0.5	0.0751	0.5	0.0644	0.85
0.0724	0.35	0.0912	0.45	0.0966	0.7	0.0992	0.55	0.161	1.05
0.120	0.85	0.187	1.9	0.193	4.4	0.147	1.5	0.354	18.85
0.217	1.7	0.381	13.4	0.289	29.45	0.244	6.55	0.740	30.85
0.410	11.95	0.767	32.3	0.676	33.05	0.437	25.25	1.32	32.75
0.797	28.7	1.347	35.25	1.062	34.85	0.823	39.05	1.90	34.1
1.376	31.15	2.12	36.9	1.642	36.25	1.306	41.15	2.673	35.2
1.956	32.3	3.086	37.2	2.512	37	2.079	41.5	3.445	35.9
2.729	32.7	4.052	37.15	3.478	37.2	3.046	41	4.412	36.2
3.695	32.75	5.018	37.1	4.44	37.3	3.818	40.55	5.185	36.3
4.854	32.8	5.308	37	5.217	37.35	5.171	39.55	5.957	36.3
6.207	32.95							6.73	36.35
								7.697	36.35
								8.856	36.45
								10.305	36.45

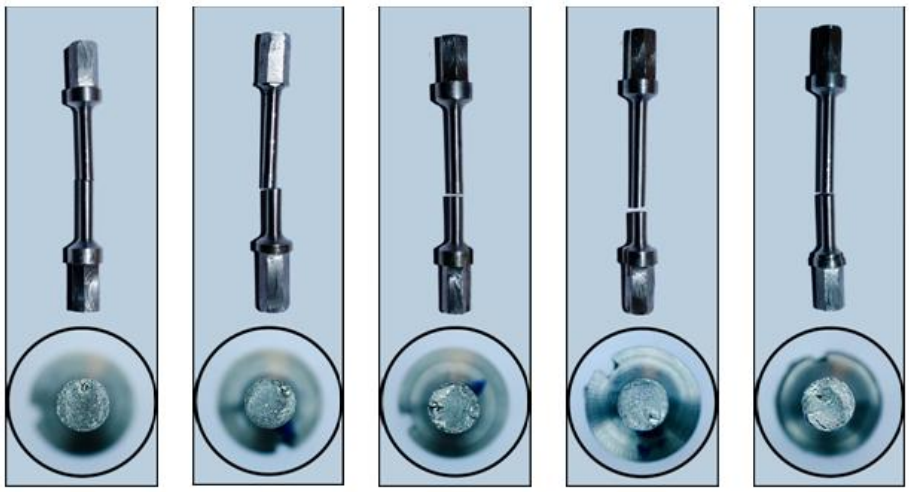

Figure 12: Rapture Location and surface for the tested Specimens The results for the two non-welded specimens ***α*** and ***β*** will be discussed first and then the discussion will advance toward the welded s p e c ime n s.

Specimen α **and** β **Results**

When testing the specimen ***α*** and ***β***, they results was of two dissimilar materials, Figure 11. The first specimen ***α*** had a higher torsional momentum resistance but went under less angular displacement before rapture. The material behavior was that of a harder and less ductile material, with a faint yield point and a maximum, ultimate, stress point, Figure 13. After the maximum stress, the curve starts to decay with a close to linear behavior until the specimen raptures at the end of the curve. The second specimen ***β*** had a lower torsional momentum resistance while being able to withstand more angular displacement before rapture. The material behavior was that of a softer an more ductile material, with an explicit yield point and a maximum stress point being the same point of rapture. This maximum is obtained before the rapture and is maintained until the specimen brakes. This hard & brittle behavior of α specimen and soft & ductile behavior of β specimen is due to the different of chemical composition in both materials. Researches has been done on the effect of chemical composition of stainless-steels on their mechanical properties [12][13]. In general,

Carbon *C***:** An increased carbon concentration caused an increase in strength and a decrease in ductility.
Silicon *Si***:** A reduction in silicon caused an increase in ductility with little effect on strength.
Phosphorus *P***:** An increase in phosphorus caused an increase in rupture life and an improvement in ductility.
Boron *B***:** An increase in boron increased rupture life and ductility.

The chemical composition analysis for Stainless-Steel α and β, Table 2 and Table 3, should that both material contained Carbon, Silicon and Phosphorus, Boron was not presented in either material. Material α had higher amount of *C*, *Si* and *P* than material β with different percentages that suggests increasing the effect of Carbon and Silicon over the effect of Phosphorus. This explains the more brittle and hard nature of α Stainless- Steel and the more soft and ductile nature of β Stainless-Steel.

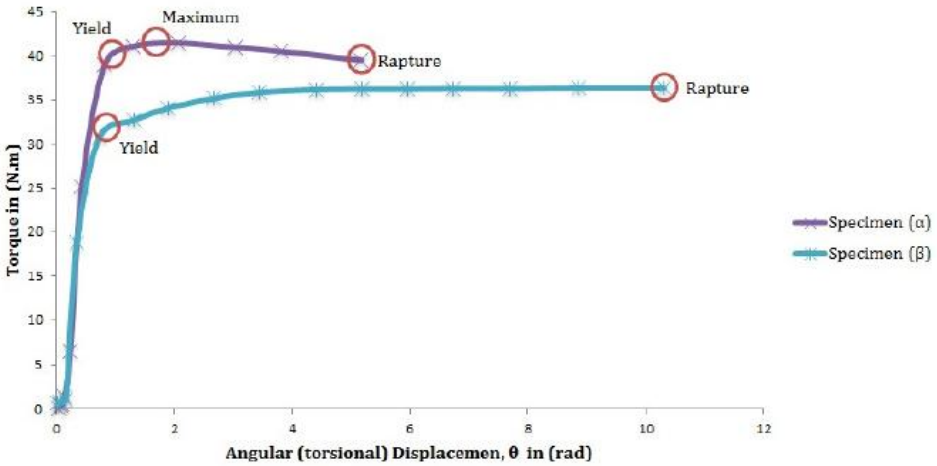

Figure 13: Torsional Displacement - Torque plot for specimens ***α*** and ***β***

Specimen 1,2 and 3 Results

Looking at the results for the welded specimens 1,2 and 3, Figure 11 and Table 7, suggested that an intermediate torsional properties for the welded joints can be achieved at increased forging pressures. Interestingly, rapture location for all specimens was not the same; however, none of the specimen broke at the location of welding, the middle of the specimen. This suggest that the exact fiction welding location was not the weak point for any specimen, and for any of the selected forging pressures; that being said, some of the specimens broke next to the welding location. This might be due to the fact that the maximum torsional stress happens at maximum distance, the middle of the specimen for each side or each material. Specimen 1, with the lowest forging pressure, had a behavior similar to material β and showed a ductility which is between α and β. However, the overall strength of the specimen was below that of both materials, the material yielded at lower applied torque and ruptured at lower applied torque. The rapture didn't happen at the welding location but happened next to it. The elastic region, the linear proportionality at the beginning of the curve, for specimen 1 had the lowest slop. This slop is an indication of how much applied torque the specimen withstand with minimum deformation; hence, specimen 1 had the lowest resistance to applied torque with minimum deformation. Specimen 2, with the intermediate forging pressure, had a behavior closer to that of material α. The ductility was lower than that of specimen 1 but the overall strength was higher than that of specimen 1 and material β, indicated by the angular displacement in Table 7. The elastic region slop had increased comparing to specimen 1 but still it was less than that of either nonwelded specimen. Specimen 3, with the highest forging pressure, behavior was, similar to specimen 2, closer to that of material α. Comparing the three specimens, the ductility for the third specimen was the lowest, but still slightly higher than the ductility of material α, while the overall strength was the higher, by a slight value comparing to specimen 2. The most important outcome of the third specimen test was the slop of the elastic region. This slop was higher than that of any of the tested specimens, including the non-welded α and β. This indicates that specimen 3 was the hardest and withstood higher applied torque with minimum deformation. Table 8 lists the rapture torque *Mrapture*, the maximum angular displacement θmax and the elastic region slop for each specimen. Figure 14 shows the relation of the three results more clearly.

Table 8: Maximum *MT max*, θmax, Elastic Region Slop

Specime	$M_{rapture}$ in$N.m$	θ_{max} inrad	Elastic
1	32.95	6.207	43.34
2	37	5.308	59.51
3	37.35	5.217	259.27
α	39.55	5.171	96.77
β	36.45	10.305	92.117

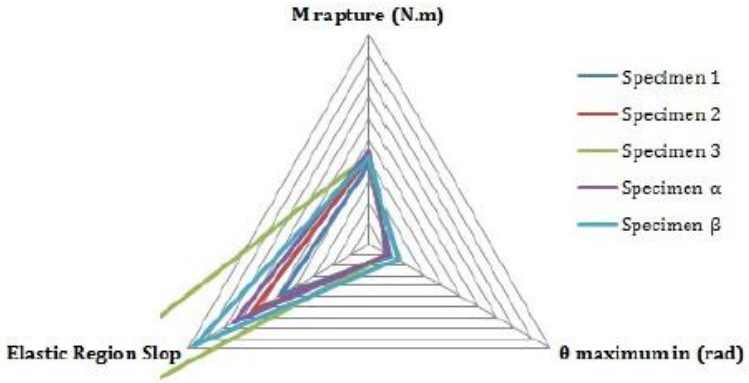

Figure 14: *Mrapture*, θmax and Elastic Region relating of the tested specimens

4.2 Simulation Results

Finite Element Analysis was used to investigate the heating and heat transfer process during the welding. The results are obtained in the form of Models and corresponding graphs. The temperature color scale for all results ranges from Blue, for minimum temperature, to Red, for maximum temperature, as shown in Figure 18.The simulation indicates that increasing the friction time will leads to an increasing in the temperature beyond the melting point of the stainless-steel. This means that increasing the friction time might lead to thin molten layers of metal between the faces in contact, even if this type of welding in considered a non-melting weld. Figure 15 shows the generating of heat between the rubbed faces and Figure 16 shows the temperature

distribution for one halve of the heated joint. The temperature keeps increasing with time and does not stop at the melting point of stainless-steel, 1400 – 1450℃. At $t = 11.5sec$, layers of both halves reach a temperature of approximately $2990C^{\circ}$; hence, molten layers of metal is presented between the two faces in contact. Figure 17 shows the radial temperature distribution across the rubbed face on one halve, the same behavior is expected or the opposite face. Each 100 simulation step represents one second of friction heating and the distribution was sensed over 1000 point along the radius, indicated on the models by $p1 - p1000$ line. Initially, the maximum temperature is sensed at the outer point of the heated surface while the minimum temperature is sensed at the center of rotation; hence, the temperature distribution is directly proportional to the radial displacement. As the friction continues, the temperature distribution gradually oppose the initial state until, eventually, the maximum temperature is sensed at the center of rotation and the minimum temperature is sensed at the outer point of the heated surface; hence, the temperature distribution is inversely proportional to the radial displacement. This

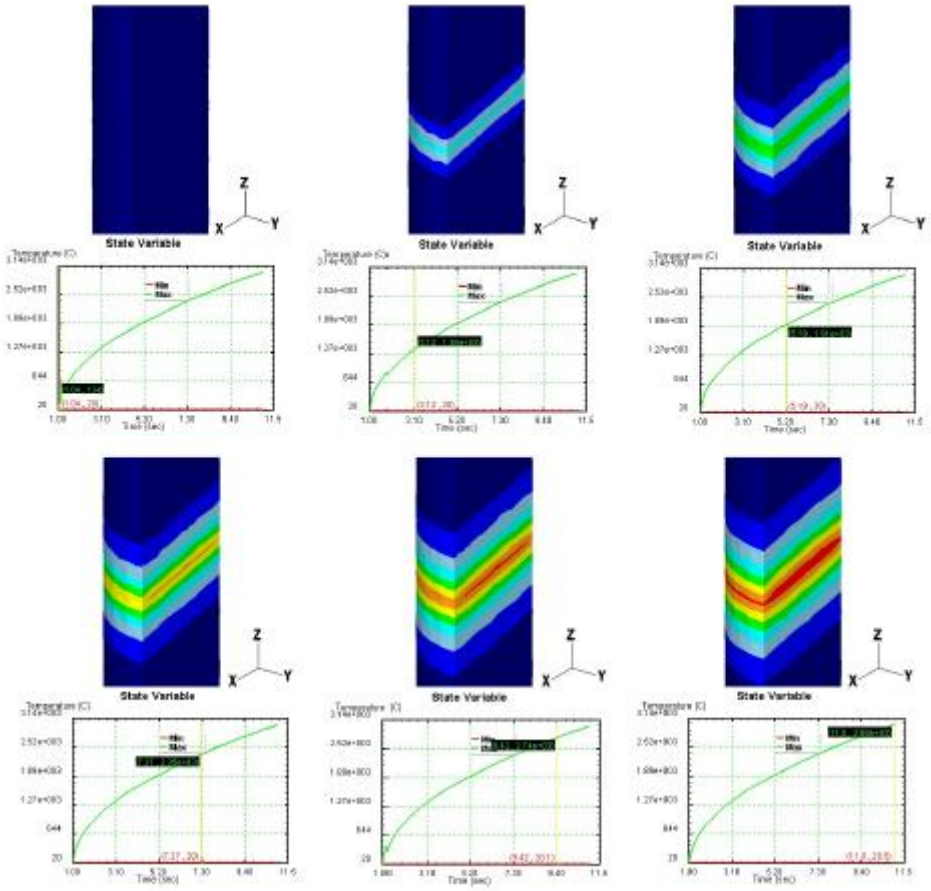

Figure 15: Frictional heating simulation results (Both Halves, Isometric Section View)

behavior is due to the combined act of heat transfer and generated heat and is divided into three stages, , Intermediate and as follows: Stage I Initially, the heat generates from the friction between the two rubbed faces. As the frictional heat is directly proportional to the frictional speed, Maximum heat is generated at the outer perimeter, where the linear velocity is maximized, and Minimum heat is generated at the center of rotation, where ideally there is no linear velocity. Stage II As the friction continues, heat is transferred from the perimeter region toward the center of rotation by conduction, according to the second law of thermodynamics, and toward the surrounding environment by convection. This means that the center gains heat while the perimeter region losses heat. Stage III Continues heat loss and heat gain at different regions will reduce the sensed temperature of the perimeter and increase the sensed temperature of the center until the initial stages is opposed. It should be noted that the third stage is to eventually change into a fourth stage of equilibrium, after welding, according to the laws of thermodynamics. From the simulation results, a heating profile for stage III was generated, Figure 18. From the profile, the sensed temperature is maximized at the core of the welding area, the center of both halves. This profile also shows that the rate of heat transfer is directly proportional to the radius.

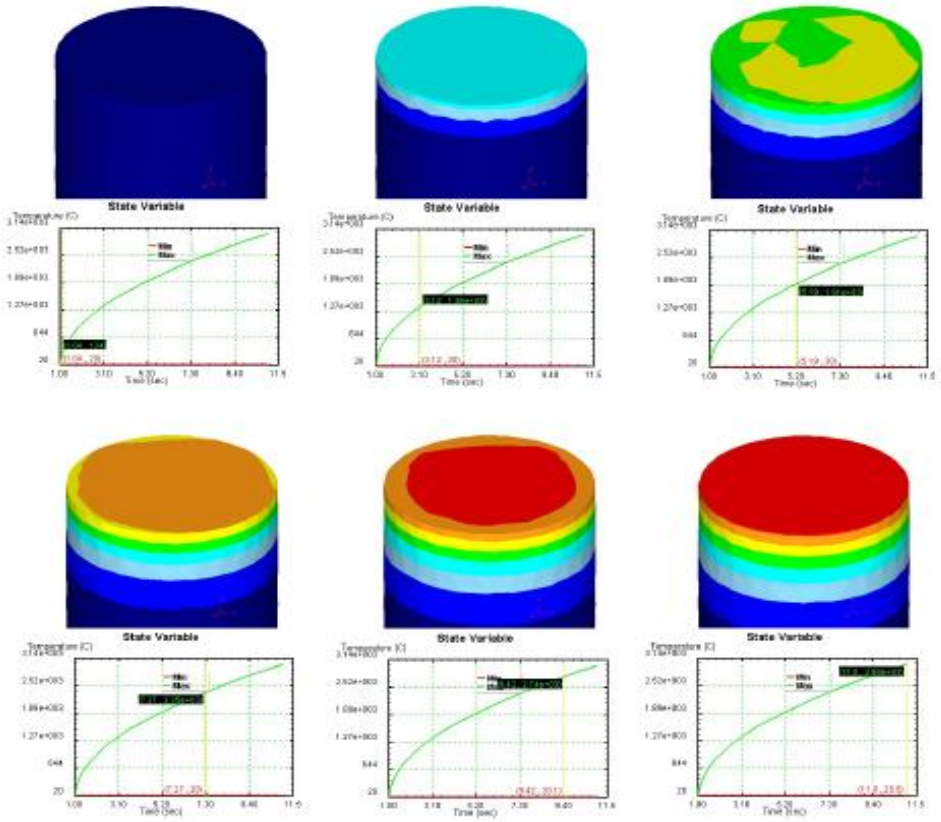

Figure 16: Frictional heating simulation results (One Halve, Isometric Top View)

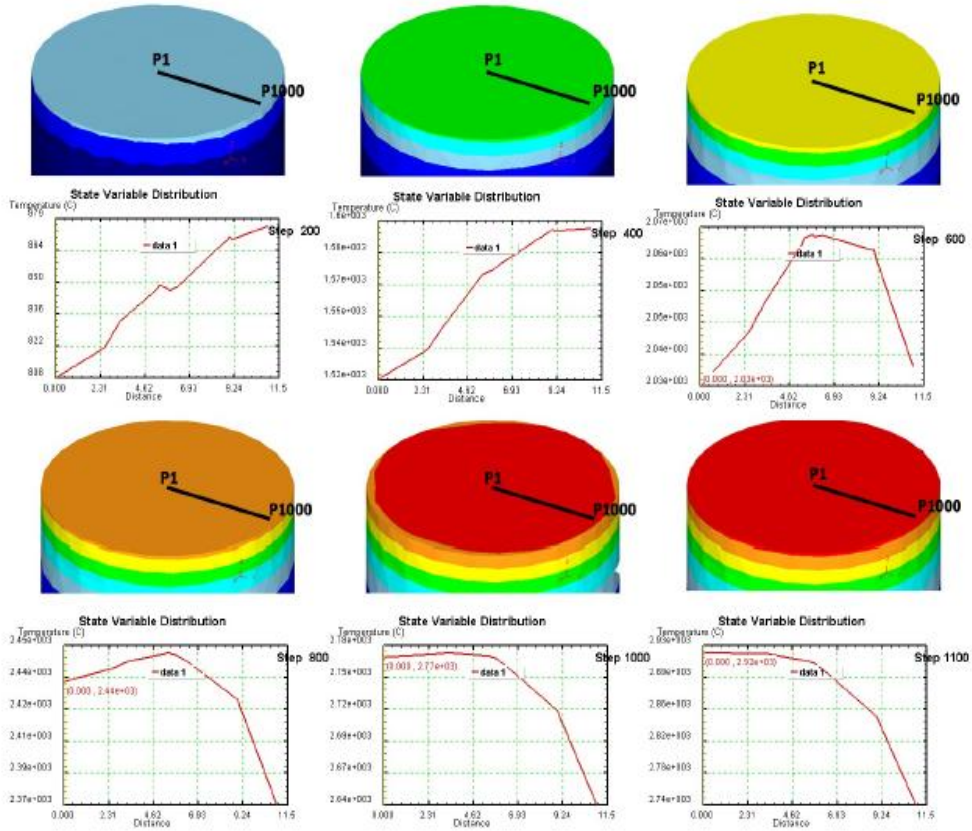

Figure 17: Frictional heating simulation results, Radial Distribution (One Halve, Isometric Top View)

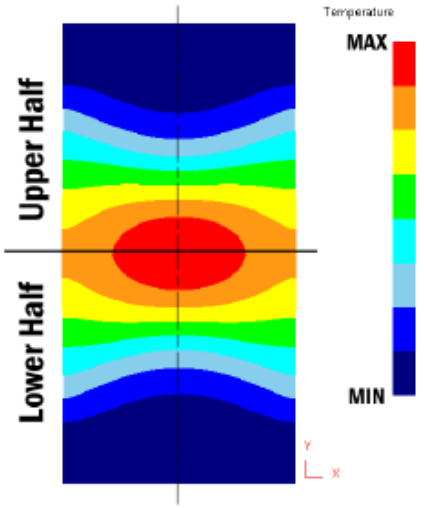

Figure 18: Frictional heating simulation results, Heating Profile (Both Halve, Front Section View)

V. Conclusions

This research investigated the effect of frictional welding between different stainless-steel materials on their torsional properties. The study was based on two main outcomes. The first was test results of specimens welded with different forging pressures. The second was the FEA of frictional heating process. Studying the obtained data, the following conclusions were reached:

1. Properly welded, the welded region has an intermediate torsional properties comparing to the welded joints.
2. The strength and brittleness of the welded region are proportional to the forging pressure.
3. Increasing the forging pressure increases the ability of withstand higher applied torque with minimum defor- mation.
4. During continues friction, the temperature keeps increasing with time, leading to thin layers of molted metal between the rubbed faces.
5. The frictional heating profile of the dubbed faces has two main stages. At the first stage, the maximum
6. temperature is sensed at the perimeter and the minimum temperature is sensed at the center. At the
7. third stage, following an intermediate stage, the maximum temperature is sensed at the center and the minimum temperature is sensed at the perimeter.
8. The maximum heat transfer occurs at the perimeter of the welded joints, while the minimum heat transfer is fond to be at the core of the welded joints.

References

[1]. Selim Sarper Yilmaz Mehmet Uzkut, Bekir Sadk Nl And Mustafa Akda. Friction Welding And Its Applications In Today's World. ,
[2]. *Friction Welding*. Mti, 1999.
[3]. Shubhavardhan Rn And Surendran S. Friction Welding To Join Dissimilar Metals. *International Journal of Emerging Technology And Advanced Engineering*, 2012.
[4]. Mmin Ahn. Friction Welding Of Different Materials. *International Scientific Conference*, 2010.
[5]. Amit Handa And Vikas Chawla. Experimental Evaluation of Mechanical Properties of Friction Welded Aisi Steels. *Cogent Engineering*, 2014.
[6]. A.B. Ismail Uday M. Basheer, M.N. Ahmad Fauzi And H. Zuhailawati. Effect of Friction Time on The Properties of Friction Welded Ysz-Alumina Composite And 6061 Aluminium Alloy. *Qatar Foundation Journals*, 2013.
[7]. Amit Handa And Vikas Chawla. An Investigation on The Effect of Axial Pressures on The Mechanical Properties of Friction Welded Dissimilar Steels. *Advances In Mechanical Engineering*, 2014.
[8]. Shear And Torsion.
[9]. Ahmet Can. Modelling of Friction Welding. *International Scientific Conference*, 2010.
[10]. Fengshou Gu Xiaocong He And Andrew Ball. A Review of Numerical Analysis of Friction Stir Welding. *Progress In Materials Science*, 2014.
[11]. L. Y. Duan By L. Fu And S. G. Du. Numerical Simulation of Inertia Friction Welding Process By Finite Element Method. *Welding Journal*, 2003.
[12]. By R. L. Klueh And D. P. Edmonds. Chemical Composition Effects on The Creep Strength of Type 308 Stainless Steel Weld Metal. *The Welding Journal*, 1986.
[13]. By R. L. Klueh And D. P. Edmonds. Chemical Composition Effects on The Creep of Type 316 And 16-8-2 Stainless Steel Weld Metal. *The Welding Journal*, 1986.